Limitation in thin-film sensing with transmission-mode terahertz time-domain spectroscopy

Withawat Withayachumnankul,[1,*] John F. O'Hara,[2] Wei Cao,[2] Ibraheem Al-Naib,[3] and Weili Zhang[2]

[1]*School of Electrical & Electronic Engineering, The University of Adelaide, Adelaide, SA 5005, Australia*
[2]*Electrical & Computer Engineering, Oklahoma State University, 202 Engineering South, Stillwater, OK 74078, USA*
[3]*Department of Physics, Engineering Physics and Astronomy, Queen's University, Kingston, ON K7L 3N6, Canada*
[*]*withawat@eleceng.adelaide.edu.au*

Abstract: Thin-film sensing with a film thickness much less than a wavelength is an important challenge in conventional transmission-mode terahertz time-domain spectroscopy (THz-TDS). Since the interaction length between terahertz waves and a sample film is short, a small change in the transmitted signal compared with the reference is considerably obscured by system uncertainties. In this article, several possible thin-film measurement procedures are carefully investigated. It is suggested that an alternating sample and reference measurement approach is most robust for thin-film sensing. In addition, a closed-form criterion is developed to determine the critical thickness, i.e., the minimal thickness of a film unambiguously detectable by transmission-mode THz-TDS. The analysis considers influences from the Fresnel transmission at interfaces and the Fabry-Pérot reflections, in addition to the propagation across the film. The experimental results show that typical THz-TDS systems can detect polymer films with a thickness down to a few microns, two orders of magnitude less than the wavelength. For reasonably accurate characterization, it is recommended that the film thickness be at least ten times above this limit. The analysis is readily extended to biomolecular and semiconductor films. The criterion can be used to estimate the system-dependent performance in thin-film sensing applications, and can help to ascertain whether an alternative terahertz sensing modality is necessary.

OCIS codes: (300.6495) Spectroscopy, terahertz.

References and links

1. W. Withayachumnankul, G. M. Png, X. X. Yin, S. Atakaramians, I. Jones, H. Lin, B. S. Y. Ung, J. Balakrishnan, B. W.-H. Ng, B. Ferguson, S. P. Mickan, B. M. Fischer, and D. Abbott, "T-ray sensing and imaging," Proc. IEEE **95**, 1528–1558 (2007).
2. K.-S. Lee, T.-M. Lu, and X.-C. Zhang, "Tera tool," IEEE Circuits Devices Mag. **18**, 23–28 (2002).
3. H.-B. Liu, G. Plopper, S. Earley, Y. Chen, B. Ferguson, and X.-C. Zhang, "Sensing minute changes in biological cell monolayers with THz differential time-domain spectroscopy," Biosens. Bioelectron. **22**, 1075–1080 (2007).
4. M. Scheller, C. Jansen, and M. Koch, "Analyzing sub-100-μm samples with transmission terahertz time domain spectroscopy," Opt. Commun. **282**, 1304–1306 (2009).

#199088 - $15.00 USD Received 7 Oct 2013; revised 27 Dec 2013; accepted 30 Dec 2013; published 9 Jan 2014

5. W. Withayachumnankul, B. M. Fischer, and D. Abbott, "Material thickness optimization for transmission-mode terahertz time-domain spectroscopy," Opt. Express **16**, 7382–7396 (2008).
6. P. U. Jepsen and B. M. Fischer, "Dynamic range in terahertz time-domain transmission and reflection spectroscopy," Opt. Lett. **30**, 29–31 (2005).
7. J. F. O'Hara, W. Withayachumnankul, and I. Al-Naib, "A review on thin-film sensing with terahertz waves," J. Infrared Millimeter Terahertz Waves **33**, 245–291 (2012).
8. W. Withayachumnankul, "Limitation in thin-film detection with transmission-mode terahertz time-domain spectroscopy" (2011), ArXiv:1111.3498v1.
9. W. Withayachumnankul, B. Fischer, H. Lin, and D. Abbott, "Uncertainty in terahertz time-domain spectroscopy measurement," J. Opt. Soc. Am. B **25**, 1059–1072 (2008).
10. Z. Jiang, M. Li, and X.-C. Zhang, "Dielectric constant measurement of thin films by differential time-domain spectroscopy," Appl. Phys. Lett. **76**, 3221–3223 (2000).
11. ISO, *Guide to the Expression of Uncertainty in Measurement (GUM)*, 1st ed. (ISO, 1993).
12. S. P. Mickan, A. Menikh, H. Liu, C. A. Mannella, R. MacColl, D. Abbott, J. Munch, and X.-C. Zhang, "Label-free bioaffinity detection using terahertz technology," Phys. Med. Biol. **47**, 3789–3795 (2002).
13. D. Hashimshony, I. Geltner, G. Cohen, Y. Avitzour, A. Zigler, and C. Smith, "Characterization of the electrical properties and thickness of thin epitaxial semiconductor layers by THz reflection spectroscopy," J. Appl. Phys. **90**, 5778–5781 (2001).
14. W. Withayachumnankul and M. Naftaly, "Fundamentals of measurement in terahertz time-domain spectroscopy," J. Infrared Millimeter Terahertz Waves (2013), accepted for publication.
15. L. Duvillaret, F. Garet, and J.-L. Coutaz, "A reliable method for extraction of material parameters in terahertz time-domain spectroscopy," IEEE J. Sel. Top. Quantum Electron. **2**, 739–746 (1996).
16. D. Grischkowsky, S. Keiding, M. van Exter, and C. Fattinger, "Far-infrared time-domain spectroscopy with terahertz beams of dielectrics and semiconductors," J. Opt. Soc. Am. B **7**, 2006–2015 (1990).
17. A. K. Azad, J. Dai, and W. Zhang, "Transmission properties of terahertz pulses through subwavelength double split-ring resonators," Opt. Lett. **31**, 634–636 (2006).
18. W. Zhang, A. K. Azad, and D. Grischkowsky, "Terahertz studies of carrier dynamics and dielectric response of n-type, freestanding epitaxial GaN," Appl. Phys. Lett. **82**, 2841–2843 (2003).
19. T. D. Dorney, R. G. Baraniuk, and D. M. Mittleman, "Material parameter estimation with terahertz time-domain spectroscopy," J. Opt. Soc. Am. A **18**, 1562–1571 (2001).

1. Introduction

Teraherz time-domain spectroscopy (THz-TDS) is an efficient tool for characterizing materials with broadband coherent terahertz radiation [1]. Typically, a femtosecond optical laser is a main component in THz-TDS. A nonlinear interaction of optical pulses with a terahertz emitter results in a burst of subpicosecond pulses spanning a range between a few hundred gigahertz and a few terahertz. The emitted pulses induce a local change in the electric field at the detector. Laser-gated detection at the detector can resolve the amplitude and phase of terahertz pulses with a high signal-to-noise ratio (SNR). In transmission measurements, the generated terahertz pulses are modified in amplitude and phase by interacting with a sample. This registered change can be used to extract the broadband complex optical constants or related quantities of the sample.

Typically, THz-TDS is used to characterize a sample that has a thickness comparable to or larger than the operating wavelength (1 THz = 300 μm). With some augmentation, the applicability of THz-TDS can be extended to thin-film sensing, where the sample thickness is much smaller than the wavelength. Example thin films include epitaxial semiconductors, dielectric insulators, and graphene, whose terahertz properties are technologically relevant in the development of high-speed circuits [2]. Biosensing is another area that THz-TDS becomes useful. Typically, a target substance or ligand establishes a thin film on top of immobilized sensing molecules. As biomolecules have characteristic responses at terahertz frequencies, the presence of the target thin layer can be detected with THz-TDS [3]. While specialized arrangements of THz-TDS are often more suited to such thin-film measurements, there are cases where characterization of the thin-film sample must be performed with the typical transmission configuration [4]. In these cases it is important to understand the measurement limitations.

For free-space transmission-mode THz-TDS, each material has an optimal thickness that

#199088 - $15.00 USD Received 7 Oct 2013; revised 27 Dec 2013; accepted 30 Dec 2013; published 9 Jan 2014

yields the lowest uncertainty in the optical constants [5]. The dynamic range of the system clearly delimits the maximum thickness of a sample that still results in valid optical parameters [6]. For a thin sample, the measurement accuracy is significantly reduced, because measurement uncertainties become relatively strong compared with a change in the amplitude and phase induced by the sample. A limitation in thin-film *characterization* exists where the film is so thin that the extracted parameters are no longer reliable [7]. Likewise, *detecting* the presence of a thin film reaches a limit when the sample is no longer distinguishable from the background material [7]. Recently, a simple criterion for determining the minimal film thickness has been proposed with its application limited to freestanding films [8].

This article includes an evaluation of three different procedures for thin-film measurement using conventional THz-TDS. Because the system uncertainties become very influential for thin-film sensing, the measurement procedure must be carefully chosen to avoid any deceptive result. The article further provides a mathematical analysis on a limitation of free-space THz-TDS for thin-film *detection*. The analysis covers common thin-film configurations, including substrate-backed films and freestanding films. By considering major physical factors of the film-wave interaction, the analysis defines the critical film thickness as a function of the system SNR and the sample refractive index. The derivable closed-form condition is useful as a rule of thumb in estimating the reliability of a THz-TDS system. It also suggests when other advanced measurement techniques are necessary to sense particular film samples.

2. Thin-film measurement procedures

Several measurement procedures have been implemented for measuring dielectric samples with THz-TDS. Generally, these procedures can, to some extent, alleviate random and systematic errors in the measurement. The sources of random error include laser intensity fluctuation, optical and electronic noise, jitter in the delay stage, sample relocation, etc., whilst the sources of systematic error include registration error, mechanical drift, etc. [9]. For thin-film sensing, these errors become relatively strong. In the *worst case*, the systematic error that progresses linearly over time might be misinterpreted as the presence of a sample. It is therefore necessary to consider these measurement procedures cautiously. In this section, we qualitatively analyze the results of applying three common measurement procedures when a THz-TDS system is run without any sample present. Despite the lack of sample, the analysis further assumes (i) a linear drift in the measured response due to the systematic error and (iii) a systematic error that is much stronger than the random error.

Case 1: Measuring the same targets consecutively and then averaging. Figure 1(a) shows illustrative amplitude values from successive measurements of the reference and sample. It is clear that this measurement procedure is not suitable for thin-film sensing. Even with no actual sample for the “Sample” measurements, the linear drift still causes a significant change in the averaged amplitude profile. This large difference can be mistakenly interpreted as the presence of a sample. Therefore, this measurement procedure is inappropriate for thin-film sensing, since the drift is not properly included in the confidence interval that bounds an error-free value.

Case 2: Measuring the reference and sample pairs in series and then normalizing each pair before averaging. The procedure is illustrated in Fig. 1(b). In this case, the normalization does not eliminate the drifting effect. It rather turns the effect into some substantial value, which is not much different for each pair. The arising small confidence interval does not incorporate the linear drift. Hence, the drifting effect might still be mistakenly interpreted as an indication of the sample. Again, this analysis proves that this measurement procedure is not valid for thin-film sensing. Such a problem is much less emphasized only

#199088 - $15.00 USD Received 7 Oct 2013; revised 27 Dec 2013; accepted 30 Dec 2013; published 9 Jan 2014

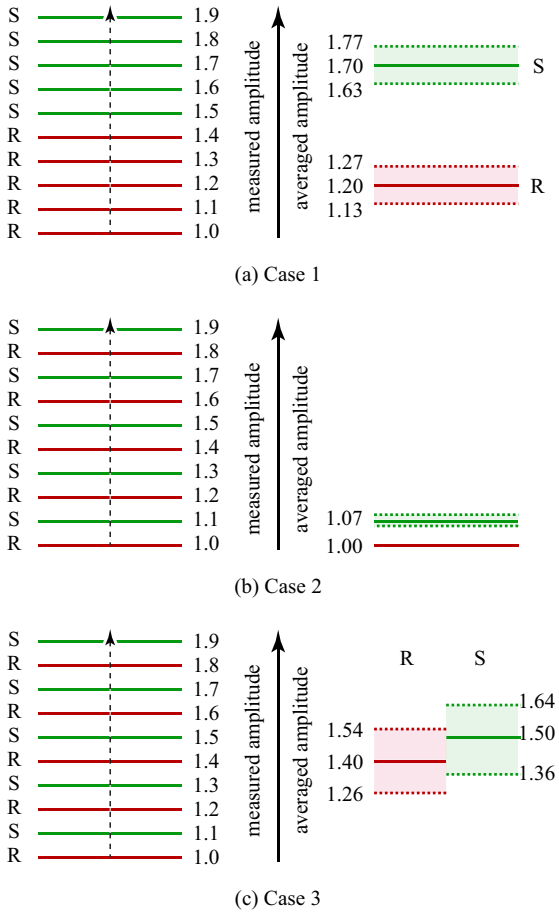

Fig. 1. Typical measurement procedures. (a) Case 1: measuring the same target consecutively and then averaging. (b) Case 2: measuring the reference and sample alternately and then normalizing each adjacent pair before averaging. (c) Case 3: measuring the reference and sample alternately and then averaging each group. The dotted arrows denote the time progress, during which a number of measurements are conducted. The letters 'R' and 'S' represent reference and sample measurements, respectively. The amplitude values are for an explanatory purpose only. The shaded areas denote the confidence intervals, which are proportional to the standard deviations.

#199088 - $15.00 USD Received 7 Oct 2013; revised 27 Dec 2013; accepted 30 Dec 2013; published 9 Jan 2014

if the swapping rate between the reference and sample is fast enough, as in the case of terahertz differential time-domain spectroscopy (DTDS) [10]. Nonetheless, the applicability of DTDS is restricted for fragile or immersed samples that do not withstand rapid mechanical oscillation.

Case 3: Measuring the reference and sample alternately and then averaging the S and R groups. In this case, as shown in Fig. 1(c), the confidence intervals for the sample and reference overlap considerably. In other words, the drifting effect is appropriately included in the confidence intervals. Detecting the presence of a sample requires that a change introduced by the sample be larger than this interval. Therefore, this measurement procedure is deemed suitable for thin-film sensing.

It can be seen that the linear drift is accounted for properly only in the last measurement procedure (case 3). As mentioned earlier, the systematic drift considered here is the worst-case scenario. It is possible that in the real measurement the drift is random, which is unlikely to cause any misleading effect. In this case, any measurement procedure is valid. However, as the nature of signal drifting is not known a priori, it is advisable to treat the problem as a worst case. In the next section the limitation of thin-film sensing is analyzed with a presumption of Case 3 measurement procedure, i.e., the error from *all the sources of uncertainty* are fully incorporated into the confidence intervals.

3. Limitation for thin-film detection

In the context of an uncertainty analysis, a confidence interval *localizes* or bounds an expected value, i.e., the value that is free from random error. In other words, the error-free value could be anywhere within this interval. Therefore, in the sample detection process, if the confidence intervals of the averaged sample and reference measurements are well separated, it can be inferred that a sample is unambiguously detected. Contrarily, if the two intervals overlap, it is possible that the two measurements share an identical expected value. Hence, in this case, the presence of a sample cannot be judged. Figure 2 schematically illustrates both of the situations. Mathematically, a confidence interval for any variable x is defined as [11]

$$\bar{x} - \frac{k_P}{\sqrt{N}} s_x \leq \mu_x \leq \bar{x} + \frac{k_P}{\sqrt{N}} s_x \,, \tag{1}$$

where $\bar{x} = \sum_{l=1}^{N} x_l / N$ is an arithmetic mean from N measurements, k_P is a coverage factor, s_x is an empirical standard deviation, and μ_x is an expected value. The coverage factor k_P of 1 defines a standard measurement uncertainty, whilst a higher value defines an expanded measurement uncertainty. If the measurement error assumes a normal probability distribution, the values $k_p = 1, 2,$ and 3 define confidence intervals with a level of confidence of 68, 95, and 99.7%, respectively. The appropriate choice depends on the criticality of the problem.

3.1. Consideration of optical constants

From Eq. (1) and the discussion in the previous paragraph, it can be established that the film sample with a complex refractive index $n_f(\omega) - j\kappa_f(\omega)$ can be distinguished from the reference material with a known index $n_0 - j\kappa_0$ by terahertz waves if either of these two criteria is satisfied:

$$\Delta n(\omega) \quad > \quad k_P \sqrt{\frac{s_{n,E_{\text{sam}}}^2}{N_{\text{sam}}} + \frac{s_{n,E_{\text{ref}}}^2}{N_{\text{ref}}} + \frac{s_{n,l}^2}{N_l}} \,, \quad \text{or} \tag{2a}$$

$$\Delta \kappa(\omega) \quad > \quad k_P \sqrt{\frac{s_{\kappa,E_{\text{sam}}}^2}{N_{\text{sam}}} + \frac{s_{\kappa,E_{\text{ref}}}^2}{N_{\text{ref}}} + \frac{s_{\kappa,l}^2}{N_l}} \,, \tag{2b}$$

#199088 - $15.00 USD Received 7 Oct 2013; revised 27 Dec 2013; accepted 30 Dec 2013; published 9 Jan 2014

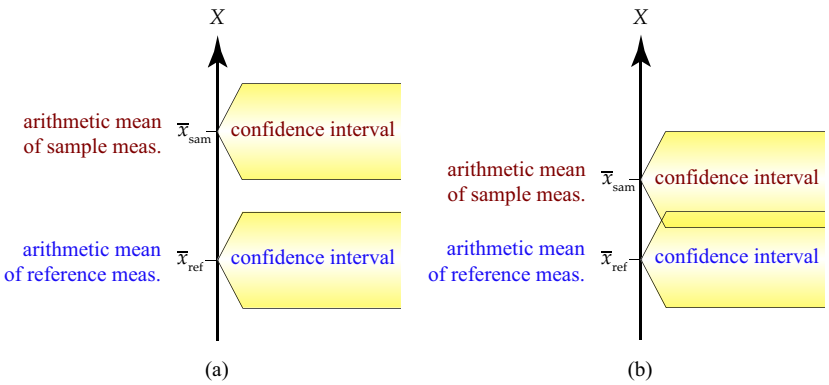

Fig. 2. Confidence intervals in the detection scheme. (a) The confidence intervals of the sample and reference measurements are well separated. The presence of a sample is confirmed. (b) The two confidence intervals partially overlap. The presence of a sample is undecided.

where $\Delta n(\omega) = \overline{n}_f(\omega) - n_0$ and $\Delta\kappa(\omega) = \overline{\kappa}_f(\omega) - \kappa_0$; $s^2_{\{n,\kappa\},E_{\rm sam}}$, $s^2_{\{n,\kappa\},E_{\rm ref}}$, and $s^2_{\{n,\kappa\},l}$ are the empirical variances of the sample optical constants caused by sample and reference signal variations, and thickness variation, respectively; $N_{\rm sam}$ and $N_{\rm ref}$ are the numbers of sample and reference measurements, respectively; and N_l is the number of sample thickness measurements. Equation (2) means that a difference between the sample refractive index or extinction coefficient and that of the reference material must be larger than the combined standard deviation, which predominately comprises two sources of random error, i.e., signal noise and drift and thickness measurement imprecision [9]. All the sources of error presumably exhibit Gaussian distributions.

The variances, $s^2_{\{n,\kappa\},l}$, could be discarded, provided that the error in thickness measurement is relatively easy to deal with or becomes irrelevant if the detection is directly based on the time-domain or frequency-domain data. Furthermore, $s^2_{\{n,\kappa\},E_{\rm sam}}$ and $s^2_{\{n,\kappa\},E_{\rm ref}}$ can be combined if the numbers of sample and reference measurements are equal. Hence, from the given assumptions, Eq. (2) can be simplified to

$$\Delta n(\omega) > \frac{k_P}{\sqrt{N}} s_n(\omega)\,, \quad \text{and} \tag{3a}$$

$$\Delta\kappa(\omega) > \frac{k_P}{\sqrt{N}} s_\kappa(\omega)\,, \tag{3b}$$

where $s^2_{\{n,\kappa\}}(\omega) = s^2_{\{n,\kappa\},E_{\rm sam}} + s^2_{\{n,\kappa\},E_{\rm ref}}$ and $N = N_{\rm sam} = N_{\rm ref}$. Typically, it can be shown that

$$\Delta n(\omega) > \Delta\kappa(\omega)\,, \quad \text{and} \tag{4a}$$

$$s_n(\omega) \leq s_\kappa(\omega)\,. \tag{4b}$$

The conditions in Eq. (4) imply that the criterion of the refractive index in Eq. (3a) is less strict than that of the extinction coefficient in Eq. (3b). In other words, to detect the presence of a sample, it is sufficient to satisfy only one criterion, Eq. (3a).

The criteria given in Eq. (3) do not contain an explicit link to the system uncertainty. In this case, it is possible to substitute $s_{\{n,\kappa\}}(\omega)$ with a standard deviation in the measured transmission spectrum as done earlier [8]. Nevertheless, the resulting criteria are approximated without considering the effect of the transmission coefficients at interfaces and the reflections inside a

#199088 - $15.00 USD Received 7 Oct 2013; revised 27 Dec 2013; accepted 30 Dec 2013; published 9 Jan 2014

sample. For a precise evaluation, an exact model relating the measured spectrum to the complex refractive index will be considered. Since the refractive index has a linear relation with the phase, the phase spectrum together with its confidence interval will be considered in Section 3.2. The analysis is supplemented by considering the limitation of film detection arising from the amplitude part, as described in Section 3.3.

3.2. Consideration of phase component

Figure 3 illustrates possible geometrical configurations for thin-film sensing. The three cases cover most common forms of thin films, including immobilized biomolecules [12], epitaxial semiconductors [13], polymers films, etc. From Fig. 3(a), the complex spectra for the reference and sample measurements can be expressed as [14], respectively,

$$E_{\mathrm{ref}}(\omega) = \tau_{as}\tau_{sa}\exp\left(-j\hat{n}_0\frac{\omega l}{c}\right)\exp\left(-j\hat{n}_s\frac{\omega l_s}{c}\right), \tag{5a}$$

$$E_{\mathrm{sam}}(\omega) = \tau_{af}\tau_{fs}\tau_{sa}\exp\left(-j\hat{n}_f\frac{\omega l}{c}\right)\exp\left(-j\hat{n}_s\frac{\omega l_s}{c}\right)\mathrm{FP}_f, \tag{5b}$$

where τ is a complex Fresnel transmission coefficient with subscripts a, f, and s for air, film, and substrate, respectively. The film has a thickness of l and a complex refractive index of $\hat{n}_f = n_f - j\kappa_f$, while the substrate has a thickness of l_s and a complex refractive index of $\hat{n}_s = n_s - j\kappa_s$. The term FP_f in the sample spectrum represents the Fabry-Pérot effect or the multiple reflections originating from the film, given as

$$\mathrm{FP}_f = \left[1 - \rho_{fa}\rho_{fs}\cdot\exp\left(-j\frac{2\hat{n}_f\omega l}{c}\right)\right]^{-1}, \tag{6}$$

where ρ_{fa} and ρ_{fs} are the complex Fresnel reflection coefficients for wave propagation from the film to free space and to the substrate, respectively. Although for thin films, these multiple reflections are not visually separable from the main pulse in the time-domain response, still their effect must be taken into account [15]. It is assumed that the reflections from the substrate are gated out. Note that Eqs. 5(a) and 5(b) are also valid for the cases in Figs. 3(b) and 3(c), for which $\hat{n}_0$ and $\hat{n}_s$ are substituted accordingly. From Eqs. 5(a) and 5(b), the transfer function of

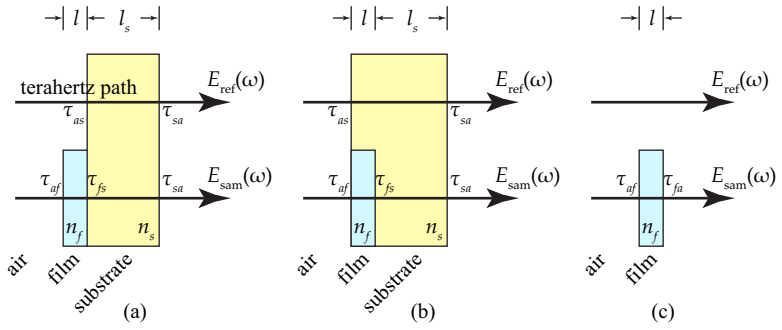

Fig. 3. Different geometries for thin-film measurement. (a) Sample on top of the substrate, typically obtained from spin coating, chemical vapor deposition, or molecular binding; $\hat{n}_0 = 1$. (b) Sample embedded in the substrate; $\hat{n}_0 = \hat{n}_s$. (c) Freestanding film; $\hat{n}_0 = \hat{n}_s = 1$. In the first two cases, the substrate is considered thick enough to allow time-gating of the internal reflections originating therein.

#199088 - $15.00 USD Received 7 Oct 2013; revised 27 Dec 2013; accepted 30 Dec 2013; published 9 Jan 2014

the thin film can be expressed as

$$\begin{aligned} H(\omega) &= E_{\text{sam}}(\omega)/E_{\text{ref}}(\omega) \\ &= \frac{\tau_{af}\tau_{fs}}{\tau_{as}} \exp\left[-j(\hat{n}_f - \hat{n}_0)\frac{\omega l}{c}\right] \text{FP}_f \,. \end{aligned} \tag{7}$$

Taking the argument of Eq. (7) yields

$$\begin{aligned} \arg(H(\omega)) &= \arg(E_{\text{sam}}) - \arg(E_{\text{ref}}) \\ &= \arg(\tau_{\text{total}}) - \Delta n\frac{\omega l}{c} + \arg(\text{FP}_f) \,, \end{aligned} \tag{8}$$

where the group of the complex Fresnel coefficients $\tau_{af}\tau_{fs}/\tau_{as}$ is combined into τ_{total}, and $\Delta n = n_f - n_0$. Equation (8) reveals that a total phase change in the transmission spectrum is caused by three different factors: the Fresnel transmission coefficients at the interfaces, the retardation inside the film, and the Fabry-Pérot effect.

In analogy to Eq. (3a), the thin film can be detected if the total phase change or the phase difference between the sample and reference measurements is larger than a geometrical combination of the corresponding confidence intervals, or

$$|\arg(E_{\text{sam}}) - \arg(E_{\text{ref}})| \;>\; k_P\sqrt{\frac{s^2_{\arg(E_{\text{sam}})}}{N_{\text{sam}}} + \frac{s^2_{\arg(E_{\text{ref}})}}{N_{\text{ref}}}} \,. \tag{9}$$

For thin-film measurement, the empirical standard deviations in the phase of the sample and reference spectra are comparable. Hence, Eq. (9) is simplified to

$$|\arg(H)| \;>\; k_P\sqrt{\frac{2}{N_{\text{ref}}}}s_{\arg(E_{\text{ref}})} \,. \tag{10}$$

Replacing the total phase change $|\arg(H)|$ by the different contributions shown in Eq. (8) results in

$$\left|\Delta n\frac{\omega l}{c} - \arg(\tau_{\text{total}}) - \arg(\text{FP}_f)\right| \;>\; k_P\sqrt{\frac{2}{N_{\text{ref}}}}s_{\arg(E_{\text{ref}})} \,. \tag{11}$$

In other words, this absolute phase change introduced by the film must be larger than the scaled standard deviation of the reference phase. For thin films where $n_f\omega l/c = 2\pi n_f \cdot l/\lambda \ll 1$, the Fabry-Pérot term can be approximated by a linear function evaluated around the origin, as detailed in Appendix A.1. Substituting the term $\arg(\text{FP}_f)$ by Eq. (23) yields

$$\left|\Delta n - 2n_f\frac{\mathscr{R}(\rho_{\text{total}})}{\mathscr{R}(\rho_{\text{total}})-1}\right|\frac{\omega l}{c} \;>\; k_P\sqrt{\frac{2}{N_{\text{ref}}}}s_{\arg(E_{\text{ref}})} \,, \tag{12}$$

where the combined complex Fresnel reflection coefficient $\rho_{\text{total}} = \rho_{fa}\rho_{fs} = \frac{\hat{n}_f-1}{\hat{n}_f+1}\cdot\frac{\hat{n}_f-\hat{n}_s}{\hat{n}_f+\hat{n}_s}$. Rearranging Eq. (12) results in the phase-based critical thickness

$$l_{c,p} \;>\; \frac{k_P}{\left|\Delta n - 2n_f\mathscr{R}(\rho_{\text{total}})/\left[\mathscr{R}(\rho_{\text{total}})-1\right]\right|}\cdot\frac{c}{\omega}\sqrt{\frac{2}{N_{\text{ref}}}}s_{\arg(E_{\text{ref}})} \,, \tag{13}$$

This condition reveals a limitation of transmission-mode THz-TDS for thin-film sensing. A sample with a thickness less than this critical thickness cannot be sensed by THz-TDS via the phase component. The condition considers the total phase change induced by the thin film

#199088 - $15.00 USD Received 7 Oct 2013; revised 27 Dec 2013; accepted 30 Dec 2013; published 9 Jan 2014

in terms of the transmission across the interfaces and the propagation and reflections inside the film itself. Note that by neglecting the phase contributions from the Fresnel transmission coefficients $\arg(\tau_{\text{total}})$ and the Fabry-Pérot reflections $\arg(\text{FP}_f)$, this condition converges to that provided in Ref [8].

To determine the critical thickness, the standard deviation $s_{\arg(E_{\text{ref}})}$ can be obtained from a set of repeated reference measurements via the Monte Carlo method after the phase of each measurement is properly unwrapped and extrapolated [14]. Since the alternating measurement procedure, Case 3 in Section 2, is employed for thin-film measurement, these reference measurements must be left out every other scan to mimic the actual condition. Increasing the number of measurements N_{ref} does not necessarily reduce the minimum sample thickness. In the situation where the long-term laser instability outweighs other random errors, the standard deviation $s_{\arg(E_{\text{ref}})}$ will be accentuated [9].

3.3. Consideration of amplitude component

As described in Section 3.1, the criterion based on the refractive index, or equivalently the phase component, is sufficient to determine the presence of a thin film. For the sake of completeness, the amplitude component is analyzed in this section. The result is a supplementary condition that defines the minimal film thickness, restricted by the uncertainty in the amplitude spectra.

The presence of a thin film can be confirmed via a change in the amplitude spectrum only if

$$|\ln|E_{\text{sam}}| - \ln|E_{\text{ref}}|| \quad > \quad k_P \sqrt{\frac{s^2_{\ln|E_{\text{sam}}|}}{N_{\text{sam}}} + \frac{s^2_{\ln|E_{\text{ref}}|}}{N_{\text{ref}}}} \,. \tag{14}$$

By assuming that $N_{\text{sam}} = N_{\text{ref}}$ and $s_{\ln|E_{\text{sam}}|} \approx s_{\ln|E_{\text{ref}}|}$, Eq. (14) is simplified to

$$|\ln|H(\omega)|| \quad > \quad k_P \sqrt{\frac{2}{N_{\text{ref}}}} s_{\ln|E_{\text{ref}}|} \,. \tag{15}$$

From Eq. (7), the amplitude component reads

$$\ln|H(\omega)| \quad = \quad \ln|\tau_{\text{total}}| - \Delta\kappa \frac{\omega l}{c} + \ln|\text{FP}_f| \,, \tag{16}$$

where $\Delta\kappa = \kappa_f - \kappa_0$. Substituting Eq. (16) into Eq. (15) gives

$$|\ln|\tau_{\text{total}}| - \Delta\kappa \frac{\omega l}{c} + \ln|\text{FP}_f|| \quad > \quad k_P \sqrt{\frac{2}{N_{\text{ref}}}} s_{\ln|E_{\text{ref}}|} \,. \tag{17}$$

Again, for $n_f \omega l/c \ll 1$, expanding the Fabry-Pérot term as shown in Appendix A.2 simplifies the condition to

$$l_{c,m} \quad > \quad \frac{k_P}{|\Delta\kappa|} \frac{c}{\omega} \sqrt{\frac{2}{N_{\text{ref}}}} s_{\ln|E_{\text{ref}}|} \,. \tag{18}$$

This condition defines the minimal thickness of a film that can be detected by observing only the transmission amplitude. The contributions to the amplitude change from the transmission at the interfaces and the etalon effects cancel each other, leaving only the effect from the absorption loss inside the film.

Both of the conditions in Eqs. (13) and (18) can be used to determine the minimal film thickness that can be detected by a system. The two conditions clearly provide different minimal thicknesses, and the applicability depends on the component of interest, i.e., the amplitude or phase. However, as discussed earlier, a thinner dielectric film can be unambiguously detected

#199088 - $15.00 USD Received 7 Oct 2013; revised 27 Dec 2013; accepted 30 Dec 2013; published 9 Jan 2014

by observing a phase change in the transmission spectrum. As for thin-film characterization, a difference in the sample amplitude or phase with respect to the reference should be at least one order of magnitude larger than the confidence interval, i.e., the film thickness for characterization should be at least ten times the minimum thickness.

4. Experiment

The proposed criteria for thin-film sensing are experimentally validated. A series of nominally identical photoresist films with different thicknesses are measured with transmission-mode THz-TDS by using the alternating reference-sample measurement procedure. The results are compared against the critical film thickness, determined from the system uncertainty.

4.1. Sample preparation, system, and measurement

The photoresist used for making the films is Shipley MICROPOSIT S1813, obtained through Rohm and Haas Electronic Materials LLC. The photoresist is spin-coated in single or multiple layers on top of a 626.6 μm thick silicon (Si) substrate with an n-type resistivity of 10 Ω-cm. Thin layers can be spin-coated in a single pass by adjusting the spin speed and duration, between 3000-4000 revolutions per minute (rpm) and 30-60 seconds duration, according to the manufacturer's specification. For films with a thickness above 2 μm, multiple spins (up to 10) are performed, and between each spin the sample is baked on a hot plate at 115°C for 60 seconds. The size of each coated-silicon sample is 12 mm$\times$24 mm, all of which is initially covered by photoresist. Then, half area of the sample is completely cleaned of photoresist to create a bare Si area to be used as a reference, as in the case shown in Fig. 3(a). This cleaning procedure uses an acetone-soaked lens tissue gently dragged in one direction across the reference area. The process is repeated several times with new tissues until the reference area of the wafer is completely clean. Four different thickness photoresist films, 0.83, 0.92, 1.10, and 2.70 μm, are precisely measured via both ellipsometry and mechanical profilometry. An extra thick photoresist film of 12.5 μm is fabricated for extracting the photoresist properties in the terahertz region. The properties of the photoresist and silicon in use are given in Appendix A.2.

A transmission THz-TDS system, shown in Fig. 4 [16, 17], is employed to characterize the photoresist properties and to study the limitation in thin-film sensing. The parabolic mirrors are arranged in 8-F confocal geometry, which provide excellent beam coupling between the transmitter and receiver. The Gaussian beam of terahertz pulses is focused to a frequency independent beam waist of 3.5 mm ($1/e$ amplitude diameter) for characterizing small samples

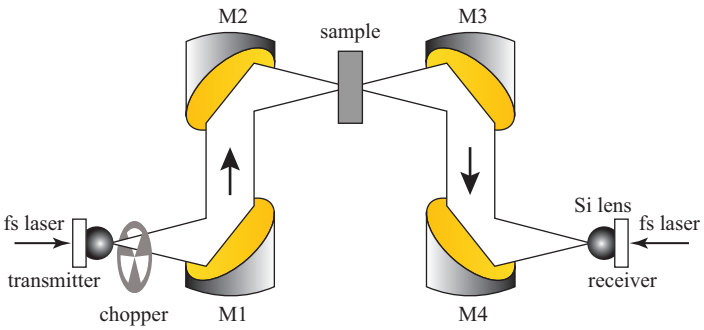

Fig. 4. Schematic diagram of modified THz-TDS setup with an 8-F confocal geometry. The notation M1,..., M4 denote the off-axis parabolic mirrors. The terahertz beam with a frequency-independent beam waist is obtained between mirrors M2 and M3.

#199088 - $15.00 USD Received 7 Oct 2013; revised 27 Dec 2013; accepted 30 Dec 2013; published 9 Jan 2014

located midway between the parabolic mirrors M2 and M3, whose effective focal length are both 50 mm. To maximally avoid film thickness variations and beam clipping artifacts, the measured sample and reference areas on the wafer are separated by only 10-15 mm, leaving a minimum of 3 mm between the edge of the terahertz beam and the edge of the photoresist sample.

The transmitter and receiver are illuminated and gated with a beam of 30 fs pulses, having an average power of 10 mW, a wavelength of 800 nm, and a repetition rate of 88 MHz. This 8-F setup is able to produce broad usable bandwidth from 0.2 to 4.5 THz. As usual, the terahertz waveform is measured by means of lock-in amplification with a time-constant of 100 ms and a point-to-point measurement delay of 300 ms. A low-noise, battery-powered, transimpedance amplifier is used ahead of the lock-in to convert the weak current signal into a stronger voltage signal. The lock-in reference is established by optical chopping, applied directly to the terahertz beam.

In all cases, the reference and sample are measured alternately in a dry air chamber. The alternating measurement procedure ensures the reliability of data for thin-film sensing, as discussed in Section 2. Both reference and sample are mounted on a remote-controlled mechanical stage so that the dry air environment is not disturbed between measurements. Each time-domain measurement, of either the sample or reference, requires about five minutes. Before further processing, the obtained temporal signals are windowed and zero-padded to remove the reflections originating inside the silicon substrate.

4.2. Validation of critical film thickness

Four reference scan datasets, where the interlacing sample scans are ignored, are utilized to determine the critical thicknesses $l_{c,p}$ and $l_{c,m}$ according to Eqs. (13) and (18). Each reference dataset with N_{ref} of 20 yields the standard deviations for the phase spectrum, $s_{\arg(E_{\mathrm{ref}})}$ and for the amplitude spectrum $s_{\ln|E_{\mathrm{ref}}|}$. In order to demonstrate the robustness of the developed models, the estimation of the critical thicknesses relies on approximated and frequency-independent optical constants $\hat{n}_f$ and $\hat{n}_s$ for the photoresist and silicon, as opposed to the exact frequency-dependent values given in Appendix A.2. Specifically, the refractive indices for the film and the silicon are fixed at $n_f = 1.6$ and $n_s = 3.4$, respectively; the silicon is treated as lossless, and the extinction coefficient for the photoresist is fixed at $\kappa_f = 0.05$. The coverage factor k_P is set to 1 for a standard measurement uncertainty.

Figure 5 illustrates two sets of the critical thicknesses, one related to the phase component and the other for the amplitude component. In Fig. 5(a) the critical thicknesses of this photoresist obtained from the phase component are reasonably constant over the usable frequency range and over different groups of scans. Beyond 4.5 THz and below 0.5 THz, the critical thicknesses ascend sharply, corresponding to a rapid decrease in the SNR of the current system. It can be deduced that this particular THz-TDS system can be used to detect thin polymer films down to about 2 μm by observing a phase change between the averaged reference and sample measurements.

On the other hand, the critical thicknesses shown in Fig. 5(b) obtained from the amplitude component vary greatly from one set of scans to the next, and vary greatly with the frequency. Interestingly, there seems to be no direct link in the trend between the amplitude- and phase-based critical thicknesses, albeit derived from the same dataset. In some datasets over a limited frequency range, the critical thickness is smaller than what is indicated by the phase component. Nevertheless, due to a strong and random variation in the critical thickness $l_{c,m}$, the amplitude component is not suitable for thin-film sensing applications.

A validation of the phase-based critical thicknesses in Fig. 5(a) is conducted by using four full sets of alternating sample and reference measurements for the four photoresist films with

#199088 - $15.00 USD Received 7 Oct 2013; revised 27 Dec 2013; accepted 30 Dec 2013; published 9 Jan 2014

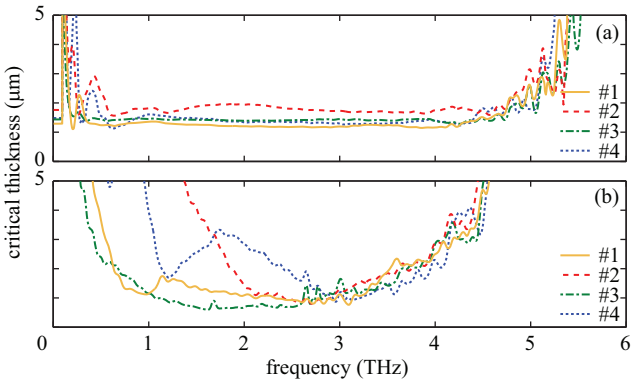

Fig. 5. Critical film thicknesses for the THz-TDS system under consideration. (a) Critical thicknesses, $l_{c,p}$, derived from the phase component of four different datasets by using Eq. (13), and (b) Critical thicknesses, $l_{c,m}$, derived from the amplitude component by using Eq. (18). The indices annotate the number designator of the dataset in use.

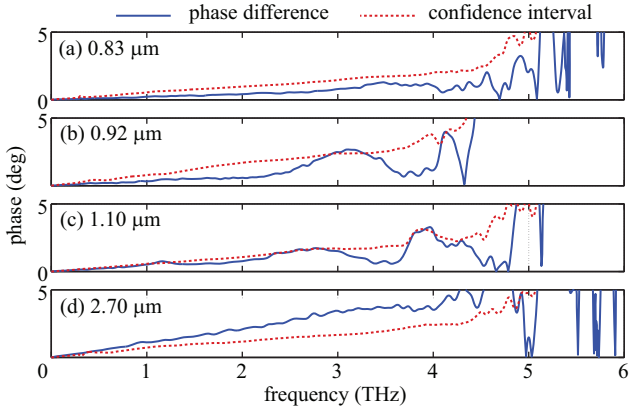

Fig. 6. Phase difference compared with confidence interval. The phase difference is obtained from the averaged sample and reference phase spectra, $|\arg(E_{\mathrm{sam}}) - \arg(E_{\mathrm{ref}})|$, and the confidence interval is from a geometrical combination of their corresponding confidence intervals, $k_P \sqrt{s^2_{\arg(E_{\mathrm{sam}})}/N_{\mathrm{sam}} + s^2_{\arg(E_{\mathrm{ref}})}/N_{\mathrm{ref}}}$, where $k_P = 1$. The numbers indicate different film thicknesses.

different thicknesses. Each film is measured to obtain 20 reference and 20 sample scans. In Fig. 6, for each film, the phase difference between the averaged sample and reference measurements is compared with the combined confidence interval. In order for the film to be detected, the condition in Eq. (9) must be satisfied, i.e., the phase difference must be larger than the combined confidence interval. It is clear from Fig. 6 that for the film thickness of 0.83 μm, the phase difference is far lower than the confidence interval. As the thickness increases to 0.92 μm and 1.10 μm, the phase difference is larger, but still below the confidence interval. For the film thickness of 2.70 μm, reasonably larger than the critical thickness of 2 μm, the phase difference overcomes the confidence interval over the usable frequency band. Thus, this film is detectable. This experiment confirms the critical thickness of 2 μm determined from the measurement uncertainty of the THz-TDS system under investigation.

#199088 - $15.00 USD Received 7 Oct 2013; revised 27 Dec 2013; accepted 30 Dec 2013; published 9 Jan 2014

Table 1. Minimum detectable film thicknesses for some common materials. The phase-based and amplitude-based minimum thicknesses $l_{c,p}$ and $l_{c,m}$ are determined by using Eqs. (13) and (18), respectively. For a substrate-backed film, the reference is assumed to be a bare substrate, as illustrated in Fig. 3(a). For a freestanding film, the reference is assumed to be free space, as in Fig. 3(c). For all the calculations, $s_{\arg(E_{\text{ref}})} = 3.2 \times 10^{-2}$ rad, $s_{\ln|E_{\text{ref}}|} = 3.8 \times 10^{-3}$, $N_{\text{ref}} = 20$, $\omega = 2\pi \times 10^{12}$ rad, and k_P = 1.

Sample	$\hat{n}_f$	n_s	$l_{c,p}$ (μm)	$l_{c,m}$ (μm)	References
Photoresist on silicon	$1.6 - 0.05j$	3.4	1.37	1.15	(this work)
Photoresist (freestanding)	$1.6 - 0.05j$	1.0	0.61	1.15	–
PDMS (freestanding)	$1.5 - 0.06j$	1.0	0.77	0.96	–
Doped GaN on sapphire	$2.7 - 0.30j$	3.0	0.31	0.19	[18, 16]

4.3. Other common thin films

The film thickness conditions given in Eqs. (13) and (18) have been experimentally validated in Section 4.2. Based on the presented experimental results, this section extends the investigation to other common thin films to gain more insight into the effect of the material properties on the minimal film thickness. The calculation assumes the standard deviations of the phase and amplitude spectra $s_{\arg(E_{\text{ref}})}$ and $s_{\ln|E_{\text{ref}}|}$ that are obtained from a reference dataset containing 20 scans or $N_{\text{ref}} = 20$. Estimated minimum detectable thicknesses of different films at 1 THz are given in Table 1. Note again that the amplitude-derived critical thicknesses, $l_{c,m}$, can vary greatly owing to a strong variation in $s_{\ln|E_{\text{ref}}|}$ from one dataset to the other, and therefore should be taken as rough estimations. All the estimated thicknesses are tied with the system described in Section 4.1, and are provided for illustrative purposes only.

Interestingly, from Table 1, it can be seen that the freestanding photoresist film lowers the phase-derived minimal thickness by half compared with the same type of film on the silicon substrate, i.e., the system is more sensitive to the freestanding film. For $2\pi n_f \cdot l/\lambda \ll 1$, the Fabry-Pérot effect from these air-film-air interfaces results in additional phase delay to enhance the phase retardation from wave propagation inside the film, whereas the air-film-silicon interfaces yield phase advancement in the Fabry-Pérot term. Compared with the photoresist, a smaller refractive index in the PDMS film leads to an increase in the phase-derived minimum thickness, and a larger absorption leads to a decrease in the amplitude-derived thickness. In the case of a doped epitaxial GaN layer, its relatively high refractive index and extinction coefficient relax the thickness constraints to only a few hundred nanometers. It can be inferred that THz-TDS detection ability is enhanced if the material under test is conducting. For characterization purposes, it is suggested that the minimal thickness should be ten times higher than these limits.

5. Conclusion

In this article, different measurement procedures commonly used for sample characterization with THz-TDS have been assessed for their suitability in thin-film sensing. It is recommended that the alternating sample and reference measurement procedure be employed to avoid misleading results. Furthermore, the critical sample thickness has been derived on the basis of the uncertainty analysis that takes into account all the possible sources of error in the system. Provided that the standard deviation of *reference* terahertz signals from a particular transmission-mode system is known a priori, the proposed model can be used to estimate the minimal film

#199088 - $15.00 USD Received 7 Oct 2013; revised 27 Dec 2013; accepted 30 Dec 2013; published 9 Jan 2014

thickness that can be detected by the system. It is revealed that the phase component is more reliable than the amplitude counterpart in detecting the sample. For polymer films with a refractive index around 1.6, the system in use can detect films with a thickness down to about 2 μm. Although the experimental validation is specific to a particular polymer, the theory is general and applicable to a wide range of films in different configurations, including epitaxial semiconductors and biomolecules. The concept of critical thickness can be readily extended to the applications of thin-film characterization.

Appendix A: Linear approximation of Fabry-Pérot term

In Sections 3.2 and 3.3, the phase and amplitude of the Fabry-Pérot function are approximated by linear functions. This section provides corresponding proofs.

A.1. Phase of the Fabry-Pérot term

The argument of the Fabry-Pérot function can be expressed as

$$\arg(\mathrm{FP}_f) \quad = \quad \arg\left[1-\rho_{\mathrm{total}}\cdot\exp\left(-jkl\right)\right]^{-1}, \tag{19}$$

where $\rho_{\mathrm{total}}=\rho_{fa}\rho_{fs}$ and $k=2\hat{n}_f\omega/c$. Evaluating the function at $l=0$ for the zeroth-order approximation yields

$$\arg(\mathrm{FP}_f)_0=-\arg(1-\rho_{\mathrm{total}})=-\arg(\tau_{\mathrm{total}}), \tag{20}$$

where $\tau_{\mathrm{total}}=\tau_{af}\tau_{fs}/\tau_{as}$. By assuming that $\hat{n}_f$ and $\hat{n}_s$ has a negligible imaginary component so that $\rho_{\mathrm{total}}\approx\mathscr{R}(\rho_{\mathrm{total}})$, Eq. (19) can be rewritten as

$$\begin{aligned}\arg(\mathrm{FP}_f) &= \arctan[\mathscr{I}(\mathrm{FP}_f)/\mathscr{R}(\mathrm{FP}_f)]\\ &\approx \arctan\left[\frac{\mathscr{R}(\rho_{\mathrm{total}})\sin kl}{\mathscr{R}(\rho_{\mathrm{total}})\cos kl-1}\right].\end{aligned} \tag{21}$$

Then, the first-order approximation can be obtained from

$$\begin{aligned}\arg(\mathrm{FP}_f)_1 &\approx l\cdot\frac{d}{dl}\arctan\left[\frac{\mathscr{R}(\rho_{\mathrm{total}})\sin kl}{\mathscr{R}(\rho_{\mathrm{total}})\cos kl-1}\right]_{l=0}\\ &\approx 2n_f\frac{\omega l}{c}\cdot\frac{\mathscr{R}(\rho_{\mathrm{total}})}{\mathscr{R}(\rho_{\mathrm{total}})-1}.\end{aligned} \tag{22}$$

Combining the two orders of approximation results in a Taylor expansion of the Fabry-Pérot phase function around the origin, or

$$\arg(\mathrm{FP}_f) \quad \approx \quad -\arg(\tau_{\mathrm{total}})+2n_f\frac{\omega l}{c}\cdot\frac{\mathscr{R}(\rho_{\mathrm{total}})}{\mathscr{R}(\rho_{\mathrm{total}})-1}. \tag{23}$$

This approximation is valid for $n_f\omega l/c=2\pi n_f\cdot l/\lambda\ll 1$.

A.2. Amplitude of the Fabry-Pérot term

The amplitude of the Fabry-Pérot part can be described as

$$\ln|\mathrm{FP}_f| \quad = \quad \ln\left|1-\rho_{\mathrm{total}}\cdot\exp\left(-jkl\right)\right|^{-1}. \tag{24}$$

Taking zeroth order approximation of Eq. (24) at $l=0$ yields

$$\ln|\mathrm{FP}_f|_0=\ln|1-\rho_{\mathrm{total}}|^{-1}=-\ln|\tau_{\mathrm{total}}|. \tag{25}$$

#199088 - $15.00 USD Received 7 Oct 2013; revised 27 Dec 2013; accepted 30 Dec 2013; published 9 Jan 2014

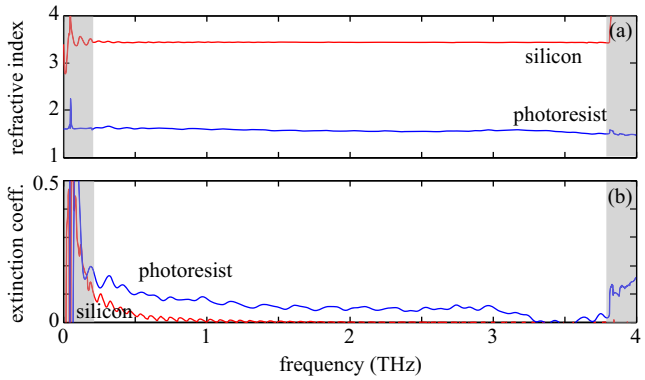

Fig. 7. Optical parameters of the photoresist and silicon. (a) Refractive index, n, and (b) extinction coefficient, κ. The shaded areas indicate unreliable parts of the data. At 1 THz, the complex refractive index for the photoresist equals $1.6-0.08j$, and the refractive index for the silicon is 3.44 with negligible loss.

Provided that the extinction coefficient in $\hat{n}_f$ is negligible, Eq. (24) can be expanded to

$$\ln|\mathrm{FP}_f| \approx -\frac{1}{2}\ln[(1-\mathscr{R}(\rho_{\mathrm{total}})\cdot\cos kl)^2+(\mathscr{R}(\rho_{\mathrm{total}})\cdot\sin kl)^2]\,. \tag{26}$$

Equation (26) can be approximated to the first order as

$$\begin{aligned}\ln|\mathrm{FP}_f|_1 &\approx l\frac{d}{dl}\left\{-\frac{1}{2}\ln[(1-\mathscr{R}(\rho_{\mathrm{total}})\cdot\cos kl)^2+(\mathscr{R}(\rho_{\mathrm{total}})\cdot\sin kl)^2]\right\}_{l=0}\\ &\approx 0\,.\end{aligned} \tag{27}$$

Hence, a Taylor expansion for the amplitude component of the Fabry-Pérot term is given as

$$\ln|\mathrm{FP}_f| \approx -\ln|\tau_{\mathrm{total}}|\,. \tag{28}$$

Again, this approximation is valid for $n_f\omega l/c \ll 1$.

Appendix B: Terahertz properties of the photoresist and silicon

The 12.5 μm-thick S1813 photoresist film on the 626.6 μm-thick silicon substrate is spin-coated and measured as described in Section 4. The silicon measurement is normalized with the free-space reference, whilst the photoresist-on-silicon measurement is normalized with the silicon reference. The optical parameters are extracted from the averaged reference and sample scans by fitting the model to the measured amplitude and phase spectra via the gradient descent method [19]. The extracted refractive index n and extinction coefficient κ for the photoresist and silicon are given in Fig. 7.

Acknowledgments

WW acknowledges financial support from the Australian Research Council (DP1095151). WC, JFO, and WZ acknowledge financial support from the US National Science Foundation (Grant No. ECCS-1232081). The authors gratefully acknowledge valuable comments from Daniel Grischkowsky, School of Electrical & Computer Engineering and the Ultrafast Terahertz Optoelectronics Laboratory, Oklahoma State University, and technical assistance of Charan M. Shah, Functional Materials and Microsystems Research Group, RMIT University, Melbourne, Victoria, Australia.

#199088 - $15.00 USD Received 7 Oct 2013; revised 27 Dec 2013; accepted 30 Dec 2013; published 9 Jan 2014